

Stratified Labeling for Surface Consistent Parallax Correction and Occlusion Completion

Jie Chen¹, Lap-Pui Chau¹, and Junhui Hou²

¹ST Engineering - NTU Corporate Lab, Nanyang Technological University, Singapore

²Department of Computer Science, City University of Hong Kong

May 29, 2022

Abstract

The light field faithfully records the spatial and angular configurations of the scene, which facilitates a wide range of imaging possibilities. In this work, we propose a LF rendering algorithm which renders high quality novel LF views far outside the range of angular baselines of the given references. A stratified rendering strategy is adopted which parses the scene contents based on stratified disparity layers and across a varying range of spatial granularities. Such stratified methodology proves to help preserve scene content structures over large perspective shifts, and it provides informative clues for inferring the textures of occluded regions. A Generative-Adversarial network model has been adopted for parallax correction and occlusion completion conditioned on the stratified rendering features. Experiments show that our proposed model can provide more reliable novel view rendering quality at large baseline expansion ratios. Over 3dB quality improvement has been achieved against state-of-the-art LF view rendering algorithms.

1 Introduction

With the commercialization of light field cameras such as Lytro [19] and Raytrix [22], light field imaging has become a popular topic and is attracting extensive research and industrial attentions. The light field (LF) is a vector function that describes the amount of light propagating in every direction through every point in space [18]. Compared with conventional 2D cameras, LF cameras can

capture extra directional information for each light ray, and such information enables exciting applications such as refocusing, 3D scene reconstruction [15, 21], material recognition [29], reflection/specularity removal [20, 24], and virtual/augment reality display [9], to just name a few.

One of the emerging applications for LF imaging is in immersive acquisition and perception of 3D environments. Compared with Conventional stereo system which uses binocular disparity for the brain to perceive the depth, LF allows to display correct scene perspectives from any viewing angles with realistic presentation of details such as shading, specularity, and focus shift etc. With the latest development of LF display technology [23, 10] that aims at achieving glasses-free and fatigue-free immersive 3-D perception, LF is now considered as a promising future media for 3-D telepresence and virtual/augmented/mixed reality applications.

For real time LF streaming based applications, one of the big technical challenges is the extremely bulky size of LF data, which requires a large data bandwidth for transmission, which could lead to content delay. This gives rises to a heated research efforts on compact representation and compression technologies of the LF data [8, 3]. Another angle of attacking this limitation is to reduce the amount of information required for the rendering of novel LF views. Numerous effects have been seen on the interpolation of densely sampled LF views based on a sparse set of inputs [14, 30, 32]. In-between views could be smoothly rendered which greatly reduces the amount of data required for transmission at real-time scenarios. Outside of view interpolation, the concept of view extrapolation

tion or baseline expansion potentially have more hope to further reduce the data requirement.

The need for an expanded LF/camera baseline is multi-fold. Firstly, it gives a wider viewing angle which provides more visual information to the viewer. Larger baselines facilitates subsequent computational procedures. Higher sub-pixel precision could be achieved for disparity estimation, more significant refocusing effect could be achieved which gives a more dramatic artistic effect. Most importantly, it gives more free-view angles for immersive perceptions, which could greatly reduce data transmission bandwidth.

In this work, we will work on the problem of rendering novel LF views that is *far* outside of the current LF baseline. Based on a given set of **LF** views with very limited angular baselines. **We** propose a stratified rendering strategy which parses the scene contents based on stratified disparity layers and across a varying range of spatial granularities. Such stratified methodology proves to help preserve scene content structures over large perspective shifts, and it provides informative clues for inferring the textures of occluded regions. A Generative-Adversarial network [7] model has been adopted for parallax correction and occlusion completion. Experiments show that our proposed model can provide more reliable novel view rendering quality especially at large baseline expansion ratios. Over 3dB quality improvement has been achieved against state-of-the-art LF view rendering algorithms.

2 Related Work

One of the most related **field** to LF baseline expansion is the interpolation of a dense LF based on a sparse set of reference inputs. Recent development in deep learning based LF reconstruction models [14, 32] have achieved far superior performance over the traditional approaches [31, 13, 26, 5]. Most notably, Kalantari et al. [14] proposed a sequential convolutional neural network (CNN) with disparity estimation and Wu *et al.* [32] proposed to use a blur-deblur scheme to counter the problem of information asymmetry between angular and spatial domain and a single CNN is used to map the blurred epipolar-plane images (EPIs) from low to high resolution.

While rendering a novel view with a large shift of viewing angle, two problems arise. First of all, the pixel

shift is much larger than interpolation problems. Which means, even small amount of inaccurate disparity estimation, which is un-noticeable for view synthesis problems, could lead to very obvious distortions when the baseline is expanded over 5 times. Therefore, an accurately estimated depth map, and the handling of feature-less regions is key for the preservation of scene structure. Recent developments of disparity estimation algorithms provides means in handling complex occlusion relationships [13, 26], and intricate scene content structures [4].

The second problem is that a lot of ambiguous regions will appear which results from occlusion and object rotation. The generative-adversarial network [7] provides successful examples in its applications in image synthesis [12, 28], and inpainting [11, 33]. Semantic labels have been used to provide content consistent outcomes. Global and locally context features have been adopted to provide a more stable and consistent inpainting. These works provide valuable inspirations to our work, in which we aim at inpainting the occluded regions with surface consistent constraints.

3 Proposed Method

Suppose we have a densely sampled 4D LF denoted as $\mathcal{L}(x, y, s, t)$ with limited baseline. (x, y) represents the spatial domain of the LF, and (s, t) represents the angular domain. A discretized LF can be considered as an array of sub-aperture images (SAI) targeted at the same scene, while sampled at slightly different viewing angles. We denote these SAIs as $\{I_n | n \in [-M, M]\}$ ($2 \times M + 1$ views in total, and I_0 denotes the central view).

Give limited angular baseline of $2 \times M + 1$, the purpose of our work is to expand the LF baseline, and render novel SAI far outside of the current view limit:

$$I_t = f(I_{-M}, \dots, I_0, \dots, I_M, t), |t| \gg M. \quad (1)$$

Here f is the function that defines the relationship between the input views $\{I_{-M}, \dots, I_M\}$ and the estimated novel SAI I_t .

Different from LF view synthesis (interpolation) or near field view extrapolation (where t is only slightly larger than M), our problem set-up in Eq. (1) is much more challenging in the following aspects:

1. The variation between views is much larger. A typical LF view synthesis problem involves pixel translation/scaling in the order of several pixels (or sub-pixels) given a set of input references. However our baseline expansion involves translation/scaling in the order of more than 10 pixels. Even a small inaccuracy in the estimation of disparity could lead to obvious structural distortions.
2. The spatial relationship between scene contents need to be more accurately and robustly modeled. Objects at different distances from the camera will have dramatically different occlusion relationships when the SAI's viewing angle has been significantly changed.
3. The handling of occluded area is much more challenging as significant changes in viewing angles could expose large un-seen areas from the reference views. How to infer the content of these occluded area based on the spatial/angular context of the reference SAIs is an important issue to be addressed.

To deal with the above-mentioned challenges, we propose a novel SAI rendering strategy based on Stratified Labeling for Surface Consistent parallax correction and occlusion completion (*SLSC*). The stratification is implemented at two levels: First, we stratify the scene into different disparity layers. For a target viewing angle from I_t , these stratified content layers are warped to the target angle independently. Finally these warped layers are fused together which represents the updated occluding relationships. Second, we segment the scene into small granularities at different sizes. When warped to the target angle at I_t , these granularities will be processed as an identical unit, which provides informative clues of *un-distorted* scene contents at each granularity level.

These intermediate outputs from stratified warping operations will be combined together as features, which will be subsequently fed into a generative network for refinement, which corrects parallax distortions, and completes occluded regions. The detail of the proposed will be discussed in this section.

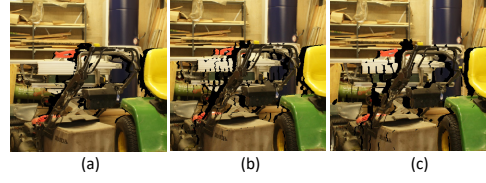


Figure 1: Comparison of warped novel views fused from stratified disparity layers in (a), and via different SP granularities in (b), and (c). Black pixels indicates ambiguous regions caused by occlusion.

3.1 Stratified Disparity Layers for Occlusion Handling

3.1.1 Layer segmentation based on disparity

With a densely sampled LF, a highly accurate disparity map with sub-pixel precision can be estimated. Recently we see obvious advancements of LF disparity estimation methods in dealing with complex content occlusion relationships [13, 27], and in processing intricate content structures [4]. We adopt a large part of the algorithm by Chen et al. [4] into our framework, since their algorithm show special advantage in preserving the disparity of intricate structures, which are most vulnerable to distortions during perspective warping. Additionally, their method also works on a superpixel granularity, which accommodates the requirements of our stratification framework.

We define the operator $\mathcal{W}(I, D)$ which warps the image I over a disparity map D . Suppose we have a disparity estimation $D_v(x, y)$, along with their per-pixel estimation confidence $C_d(x, y)$ for each input LF SAI I_v , $v = [-M, M]$ using the method from [4]. We can warp a given I_v to the target view I_t according to:

$$I_v^t(x, y) = \mathcal{W}[I_v(x, y), (t - v) \times D_v(x, y)] \quad (2)$$

$$= I_v[(x, y) + (t - v) \times D(x, y)]. \quad (3)$$

Note that the under-script v in I_v^t indicates the warping outcome is based on the input reference view of I_v .

To deal with the challenges of parallax distortion and ambiguities caused by occlusion over large perspective warping ranges, we propose to warp the image separately based on stratified disparity layers. The range of varia-

tion for $D(x, y)$ is divided into equivalent intervals. Pixels that have disparity values within the same interval are grouped as one layer Ω_k , where $k = 1, 2, \dots$, indicates the disparity level. A *stratified volume* of disparity maps $\{\mathcal{S}_v^k | k = 1, 2, \dots\}$ can be created according to:

$$\mathcal{S}_v^k(x, y) = \begin{cases} D_v(x, y) & D_v(x, y) \in \Omega_k \\ 0 & \text{otherwise.} \end{cases} \quad (4)$$

A volume of warped novel SAIs $\{I_v^{t,k}\}$ can be calculated based on different input references v and different stratified disparity layers k according to:

$$I_v^{t,k} = \mathcal{W}(I_v(x, y), (t - v) \times \mathcal{S}_v^k) \quad (5)$$

3.1.2 Layer Volume Fusion

Given the volume of warped views $\{I_v^{t,k}\}$, a fused novel view will be calculated that combines the occlusion relationships and inter-view dependencies. Starting from disparity layer k_0 that corresponds to the *furthest* scene distance ranges, the warped pixels from $\{I_v^{t,k_0}\}$ will occupy the pixels of \tilde{I}_v^t . Subsequently, nearer layers will be processed accordingly. When there is a pixel occupation conflict, nearer layers will always replace the pixels from further layers.

After combing the stratified layers, we have a volume of novel view rendering based on every reference input views $\{\tilde{I}_v^t | v = -M, \dots, M\}$. Each \tilde{I}_v^t is largely similar to each other however each contains slightly different complementary perspective information around the occlusion borders. They are combined to provide the most informative rendering feature

$$\tilde{I}^t = \text{mean}_v \tilde{I}_v^t \quad (6)$$

We defined the layer fusion operator $\mathcal{F}_k[\cdot]$ that renders a novel view based on the layer occlusion occupation priority and the combination of all input reference views as introduced in this section, we have:

$$\tilde{I}^t = \mathcal{F}_{k,v} [I_v^{t,k}] \quad (7)$$

Due to unavoidable disparity estimation inaccuracies, there could show obvious distortions and occlusion gaps especially when t is large, as demonstrated in Fig. 1.

3.2 Stratified Spatial Granularity for Warping Distortion Correction

In order to prevent content distortion and preserve structural consistency over large ranges of parallax warping, we propose to warp the target scenes based on different granularity levels based on units of superpixels.

The concept of SP is to group pixels into perceptually meaningful atomic regions [1, 25, 17]. Boundaries of SP usually coincide with those of the scene contents. The SPs are very adaptive in shape, and are more likely to segment uniform depth regions compared with rectangular units. We implement SP segmentations on the central view I_0 at multiple SP scales (different SP scales correspond to different pixel numbers within each SP). Smaller SPs provides finer granularity that better binds to intricate object structures, while SPs with larger granularity prevent distortion over large, and textureless scene regions.

A pixel-wise disparity map $D_p^l(x, y)$ can be calculated as the median of confident pixels and regularized as introduced in [4]. The superscript l indicates the SP level. During warping, all pixels within the same SP share identical disparity value. and therefore, they remain the same outlook after perspective warping.

Based on $D_p^l(x, y)$, a volume of stratified disparity maps can be calculated as:

$$\mathcal{P}^{l,k} = \begin{cases} D_p^l(x, y) & D_p^l(x, y) \in \Omega_k \\ 0 & \text{otherwise.} \end{cases} \quad (8)$$

here l is the superpixel granularity level. Different l indicates different operational units. The warping process to the target view follows the same procedures as introduced in Seg. 3.1, with the difference that operation works on all pixels within the same SP equally.

$$I_0^{t,l,k} = \mathcal{W}[I_0(x, y), t \times \mathcal{P}^{l,k}]. \quad (9)$$

Based on Eq. (9), the central view can be warped to the target view based on different SP levels k , and finally fused as novel rendering volumes of $\{\hat{I}^{t,l}\}$:

$$\hat{I}^{t,l} = \mathcal{F}_k [I_0^{t,l,k}] \quad (10)$$

In our implementation, we set up 2 SP levels each with 100 and 400 pixels per SP, respectively.

3.3 Surface Consistent Features

On top of RGB values, the disparity maps are also warped into the target view according to:

$$D^t(x, y) = \mathcal{F}(\mathcal{S}_v^k(x, y)) \quad (11)$$

This warped disparity map will be quantized into discrete labels according to:

$$D_L^t(x, y) = k, \text{ if } D^t(x, y) \in \Omega_k \quad (12)$$

Both in \tilde{I}^t , $\hat{I}^{t,l}$ and $D_L^t(x, y)$, there exist large areas of ambiguous regions caused by occlusion and warping. Since it is theoretically much easier to inpaint the ambiguous regions on the disparity map than RGB values. We propose a procedure for the inpainting of rendered disparity map D_L^t so that it can be used to guide the subsequent inpainting process of the RGB image. We adopt a classic image morphological dilation operator which propagates larger values (which corresponds to more distant surfaces) within a local window to the zero marked ambiguous pixels. The dilation operator is based on the simple while efficient logic that *any regions of ambiguity belongs to its furthest-away local surface*.

With D_L^t as *surface consistent* guide, it can potentially instruct subsequent RGB inpainting modules which surface the ambiguous region belongs to, such that relevant structural and textural features could be retrieved exclusively from the correct reference surface without distortion the occlusion boundaries.

3.4 Generative-Adversarial Network for Parallax Correction and Occlusion Completion

3.4.1 Parallax Correction and Occlusion Completion Network

The parallax correction and occlusion completion (*PCOC*) network is based on a fully convolutional network. An overview of the network structure is shown in Fig. 2. The input of the *PCOC* network is the RGB images of $\tilde{I}_v^t(x, y)$, $\{\hat{I}_0^{t,l}\}$, and the label guiding map

$$D_L^t(x, y).$$

$$\begin{aligned} \mathcal{T}_1(x, y) &= \hat{I}^{t,1}(x, y) - \tilde{I}^t(x, y), \mathcal{T}_1 \in \mathbb{R}^{W \times H \times 3}, \\ \mathcal{T}_2(x, y) &= \hat{I}^{t,2}(x, y) - \tilde{I}^t(x, y), \mathcal{T}_2 \in \mathbb{R}^{W \times H \times 3}, \\ \mathcal{T}_3(x, y) &= D_L^t(x, y) - 0.5, \mathcal{T}_3 \in \mathbb{R}^{W \times H \times 1}. \end{aligned}$$

Here $W = H = 128$ is the spatial patch size. The input feature is $\{\mathcal{T}_1, \mathcal{T}_2, \mathcal{T}_3\} \in \mathbb{R}^{W \times H \times 7}$. The output is an RGB image $\hat{I}^t \in \mathbb{R}^{W \times H \times 3}$. Note that the surface consistent map $D_L^t(x, y)$ has been normalized to the range of $[0, 1]$.

The occlusion gaps are zero valued in \mathcal{T}_1 , \mathcal{T}_2 and \mathcal{T}_3 , therefore it serves as an indicator to the *PCOC* network concerning which pixel areas to carry out *occlusion completion*, and which areas to impose *parallax correction*.

The general architecture of *PCOC* follows an encoder-decoder structure, which allows to reduce the memory usage and computational time by initially decreasing the resolution before further processing the image. Afterwards, the output is restored to the original resolution using deconvolution layers.

3.4.2 Context Discriminator

The context discriminator is based on convolutional neural networks that compress the image into small feature vectors. Outputs of the networks are continuous value corresponding to the probability of the rendered novel view \hat{I}^t being real. An overview of the networks can be seen in Fig. 2.

3.4.3 Training Details

We used the MPI Light Field Archive [2] for the training as well as evaluation of our model. The archive consists of 9 synthetic and 5 captured real-world scenes. All of the 14 LF data has a large angular base-line of 101 views, which allows enough angular flexibility to train our model.

We have chosen the 9 center views (view index range 47 to 55 out of the 101 views) were used as input reference, the side views with index range 11 to 31 and 71 to 91 were used as ground truth for baseline expansion. Note that since the input LF baseline radius is $\frac{9-1}{2} = 4$,

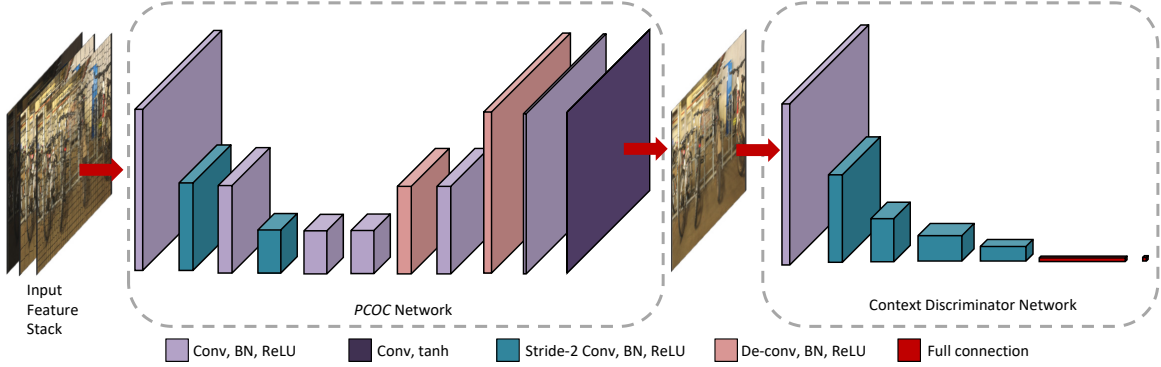


Figure 2: Network structure for the proposed *PCOC-Net*.

therefore view 11 and view 71 corresponds to an angular baseline expansion rate of 10x; and view 31 and 71 correspond to 5x, respectively.

In order to train the network such that inpainting of occlusion areas, and the parallax correction areas are realistic looking, two loss functions are jointly used: a L_1 loss term \mathcal{L}_{L_1} for content fidelity between the rendered novel view \hat{I}^t and the ground truth view, and a Generative Adversarial Network (GAN) [7] loss \mathcal{L}_{GAN} to improve the realism of the results. The final objective is:

$$\mathcal{L} = \mathcal{L}_{L_1} + \lambda \mathcal{L}_{GAN}. \quad (13)$$

To optimize our networks, We used stochastic gradient descent (SGD) to minimize the objective functions. We alternated between one gradient descent step on the generative *PCOC* net, and then one step on the context discriminator net. Mini-batch size is set as 20 for better trade-off between speed and convergence. The Xavier approach [6] is used for network initialization, and the ADAM solver [16] is adpatoed for system training, with parameter settings $\beta_1 = 0.9$, $\beta_2 = 0.999$, and learning rate $\alpha = 0.0001$. Following suggestions from [11], we train the *PCOC* net 1000 epochs, and then start the alternating training with the discriminator.

4 Model Evaluation

We evaluate our *SLSC* model both quantitatively and qualitatively and compare its performance with state-of-the-art methods in this section. Three methods were chosen

for comparison: the spatial-angular alternating filtering algorithm (*SAA-ECCV18*) [34], the learning based view synthesis algorithm (*LVS-TOG16*) [14], and a direct warping algorithm based on disparity maps estimated based on superpixel regularization over partially occluded border regions (*POBR-TIP18*) [4]. Note that both *SAA-ECCV18* and *LVS-TOG16* were originally designed for LF view interpolation give a sparsely sample reference inputs. Both of them have been retrained over the MPI dataset for the purpose of baseline expansion (extrapolation). 4 interleaved layers have been adopted for *SAA-ECCV18*. 9 adjacent center views (view index range from 47 to 55) were selected as input reference for both networks, and side views of index range 11 to 31, and 71 to 91 were used as ground truth for training, which represents angular baseline expansion limits from 5x to 10x.

Another baseline method is also chose for comparison, in which we used $\{\mathcal{T}_1, \mathcal{T}_2\}$ as input feature to the *PCOC* network, without the surface consistent guide $\{\mathcal{T}_3\}$. This baseline was used to access the importance of the surface consistency feature in the rendering of novel views. We denote this method as *SL* (without Surface Consistency feature SC).

Four scenes, which include 2 real-world scenes *Bikes* and *Workshop*, and 2 synthetic scenes *ArtGallery2zoom* and *Furniture1* were used as the testing dataset, the rest 9 scenes were used for model training.

Table 1: Rendering quality for different algorithms at different baseline expansion ratios.

| Testing Data | Expan. Ratio | LVS-TOG16 [14] | | SAA-ECCV18 [34] | | POBR-TIP18 [4] | | SL (w/o SC) | | SLSC | |
|-------------------|--------------|----------------|------|-----------------|------|----------------|------|-------------|------|-------|------|
| | | PSNR | SSIM | PSNR | SSIM | PSNR | SSIM | PSNR | SSIM | PSNR | SSIM |
| Art Gallery2 zoom | 5 | 19.02 | 0.82 | 23.17 | 0.85 | 22.60 | 0.89 | 24.42 | 0.91 | 28.35 | 0.92 |
| | 7 | 18.25 | 0.80 | 19.76 | 0.81 | 20.70 | 0.87 | 22.92 | 0.89 | 25.38 | 0.90 |
| | 9 | 17.13 | 0.76 | 17.93 | 0.78 | 19.36 | 0.85 | 20.558 | 0.87 | 23.28 | 0.87 |
| Bikes | 5 | 18.90 | 0.69 | 23.75 | 0.59 | 22.94 | 0.80 | 25.37 | 0.86 | 26.87 | 0.88 |
| | 7 | 18.49 | 0.64 | 21.52 | 0.66 | 21.23 | 0.74 | 24.23 | 0.83 | 25.48 | 0.83 |
| | 9 | 17.98 | 0.59 | 19.93 | 0.73 | 20.12 | 0.69 | 22.54 | 0.78 | 23.85 | 0.78 |
| Furniture1 | 5 | 26.72 | 0.96 | 34.56 | 0.96 | 29.06 | 0.97 | 30.12 | 0.97 | 31.11 | 0.98 |
| | 7 | 26.45 | 0.95 | 32.05 | 0.95 | 28.12 | 0.96 | 29.50 | 0.97 | 30.29 | 0.97 |
| | 9 | 24.88 | 0.92 | 28.91 | 0.93 | 27.27 | 0.95 | 28.44 | 0.96 | 29.30 | 0.96 |
| Workshop | 5 | 19.89 | 0.78 | 26.36 | 0.82 | 24.32 | 0.91 | 26.76 | 0.94 | 30.30 | 0.95 |
| | 7 | 19.26 | 0.72 | 23.29 | 0.75 | 22.56 | 0.86 | 25.82 | 0.93 | 28.03 | 0.92 |
| | 9 | 18.00 | 0.65 | 20.66 | 0.64 | 21.32 | 0.82 | 23.77 | 0.89 | 26.46 | 0.89 |

4.1 Quantitative Evaluation

We quantitatively evaluate the PSNR (Peak signal-to-Noise Ratio) and SSIM (Structural Similarity Index) of rendered novel views. Tbl. 1 shows the results for the four testing scenes at different baseline expansion ratios of 5, 7, and 9 respectively. Additionally, the average PSNR for all the testing data have been plotted as curves for each competing method in Fig. 3.

As can be seen, our proposed *SLSC* model provides a consistent 2-5 dB advantage over all competing methods. The advantage is especially large at larger baseline expansion ratios.

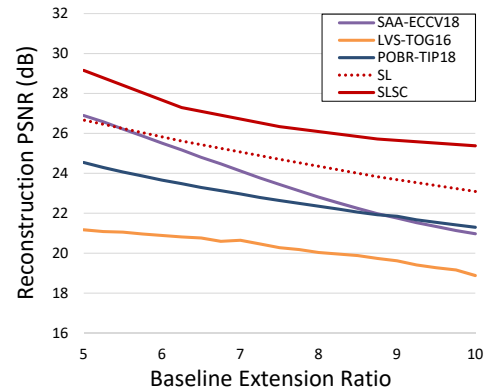


Figure 3: CNN architecture for compensation of misalignment blur. Each convolutional layer is followed by a rectified linear unit (ReLU).

4.2 Qualitative Evaluation

We visually compare the quality of rendered novel views from our method, and compare it with different methods.

Fig. 4 shows the output from the *PCOC*-Net based on the input stratified shifted features. As we can see that the gaps caused by occlusion and perspective shifting has been corrected/predicted satisfactorily. With the input surface consistent map as guide, the *PCOC*-Net produces more stable and surface consistent inpainting outcomes as highlighted in Fig. 5. The example on the top row of Fig. 5 highlights how the *PCOC* net corrects the parallax distortions. Note how the width of the chair legs have been restored to normal on the last column. As can be seen,

SL tend to produce blurred and incorrect predictions at the disparity borders. More visual comparisons are give in Fig. 6, as can be seen that the rendered novel views from our proposed *SLSC* model provides the highest quality outputs, while other competing methods show obvious blur and errors over large parallax changes.

4.3 Discussion

LF baseline expansion is a challenging problem. The key to high quality rendering is an accurate estimation of scene depth. It is challenging for even state-of-the-art methods at intricate and/or textureless regions. LF view synthesis modeled re-trained for this task proves to perform poorly mainly because the content variation is much more drastic than view interpolation problems, and it requires accurate estimation of scene structures in order to preserve it well from another drastically different viewing angle. We believe our stratified analysis methodology has high potential for further improvement when it is combined with of structure level understanding of scene geometry.

5 Concluding Remarks

We have proposed a LF rendering algorithm based on a given set of IF views with very limited angular baselines. Stratified rendering strategy is adopted which parses the scene contents based on different disparity segments and based on different spatial granularities. Such stratified methodology proves to help preserve scene content structures over large perspective shifts, and it provides informative clues for inferring the textures of occluded regions. A generative-adversarial model has been adopted for parallax correction and occlusion completion. Experiments show that our proposed model can provide more reliable novel view rendering quality especially at large baseline expansion ratios. Over 3dB quality improvement has been achieved against state-of-the-art LF view rendering algorithms.

References

- [1] R. Achanta, A. Shaji, K. Smith, A. Lucchi, P. Fua, and S. Susstrunk. Slic superpixels compared to state-of-the-art superpixel methods. *IEEE Transactions on Pattern Analysis and Machine Intelligence*, 34(11):2274–2282, 2012. [4](#)
- [2] V. K. Adhikarla, M. Vinkler, D. Sumin, R. Mantiuk, K. Myszkowski, H.-P. Seidel, and P. Didyk. Towards a quality metric for dense light fields. In *Proceedings of the IEEE Conf. on Computer Vision and Pattern Recognition (CVPR)*, 2017. [5](#)
- [3] J. Chen, J. Hou, and L. P. Chau. Light field compression with disparity-guided sparse coding based on structural key views. *IEEE Transactions on Image Processing*, 27(1):314–324, Jan 2018. [1](#)
- [4] J. Chen, J. Hou, Y. Ni, and L. Chau. Accurate light field depth estimation with superpixel regularization over partially occluded regions. *IEEE Transactions on Image Processing*, 27(10):4889–4900, Oct 2018. [2](#), [3](#), [4](#), [6](#), [7](#)
- [5] J. Chen, J. Hou, Y. Ni, and L.-P. Chau. Accurate light field depth estimation with superpixel regularization over partially occluded regions. *arXiv preprint arXiv:1708.01964*, 2017. [2](#)
- [6] X. Glorot and Y. Bengio. Understanding the difficulty of training deep feedforward neural networks. In *International Conference on Artificial Intelligence and Statistics*, pages 249–256, 2010. [6](#)
- [7] I. Goodfellow, J. Pouget-Abadie, M. Mirza, B. Xu, D. Warde-Farley, S. Ozair, A. Courville, and Y. Bengio. Generative adversarial nets. In *Advances in neural information processing systems*, pages 2672–2680, 2014. [2](#), [6](#)
- [8] J. Hou, J. Chen, and L. P. Chau. Light field image compression based on Bi-level view compensation with rate-distortion optimization. *IEEE Transactions on Circuits and Systems for Video Technology*, pages 1–1, 2018. [1](#)
- [9] F.-C. Huang, K. Chen, and G. Wetzstein. The light field stereoscope: Immersive computer graphics via factored near-eye light field displays with focus cues. *ACM Transactions on Graphics*, 34(4):60:1–60:12, July 2015. [1](#)
- [10] F.-C. Huang, K. Chen, and G. Wetzstein. The light field stereoscope: immersive computer graphics via factored near-eye light field displays with focus cues. *ACM Transactions on Graphics (TOG)*, 34(4):60, 2015. [1](#)
- [11] S. Iizuka, E. Simo-Serra, and H. Ishikawa. Globally and locally consistent image completion. *ACM Transactions on Graphics*, 36(4):107, 2017. [2](#), [6](#)
- [12] P. Isola, J.-Y. Zhu, T. Zhou, and A. A. Efros. Image-to-image translation with conditional adversarial networks. *arXiv preprint*, 2017. [2](#)
- [13] H.-G. Jeon, J. Park, G. Choe, J. Park, Y. Bok, Y.-W. Tai, and I. So Kweon. Accurate depth map estimation from a lenslet light field camera. In *IEEE Conference on Computer Vision and Pattern Recognition*, pages 1547–1555, 2015. [2](#), [3](#)
- [14] N. K. Kalantari, T.-C. Wang, and R. Ramamoorthi. Learning-based view synthesis for light field cameras. *ACM Transactions on Graphics*, 35(6):193, 2016. [1](#), [2](#), [6](#), [7](#)
- [15] C. Kim, H. Zimmer, Y. Pritch, A. Sorkine-Hornung, and M. H. Gross. Scene reconstruction from high spatio-

- angular resolution light fields. *ACM Transactions on Graphics*, 32(4):73–1, 2013. 1
- [16] D. Kingma and J. Ba. Adam: A method for stochastic optimization. *arXiv preprint arXiv:1412.6980*, 2014. 6
- [17] Z. Li and J. Chen. Superpixel segmentation using linear spectral clustering. In *IEEE Conference on Computer Vision and Pattern Recognition*, pages 1356–1363, June 2015. 4
- [18] G. Lippmann. La photographie intégrale. *Academie des Sciences*, 146:446–451, 1908. 1
- [19] R. Ng, M. Levoy, M. Brédif, G. Duval, M. Horowitz, and P. Hanrahan. Light field photography with a hand-held plenoptic camera. *Computer Science Technical Report CSTR*, 2005. 1
- [20] Y. Ni, J. Chen, and L.-P. Chau. Reflection removal based on single light field capture. In *IEEE International Symposium on Circuits and Systems*, 2017. 1
- [21] C. Perra, F. Murgia, and D. Giusto. An analysis of 3D point cloud reconstruction from light field images. In *IEEE International Conference on Image Processing Theory Tools and Application*, pages 1–6, 2016. 1
- [22] C. Perwass and L. Wietzke. Single lens 3d-camera with extended depth-of-field. In *Human Vision and Electronic Imaging*, volume 17, pages 829108–829108–15, 2012. 1
- [23] A. Stern, Y. Yitzhaky, and B. Javidi. Perceivable light fields: Matching the requirements between the human visual system and autostereoscopic 3-d displays. *Proceedings of the IEEE*, 102(10):1571–1587, Oct 2014. 1
- [24] M. W. Tao, J.-C. Su, T.-C. Wang, J. Malik, and R. Ramamoorthi. Depth estimation and specular removal for glossy surfaces using point and line consistency with light-field cameras. *IEEE Transactions on Pattern Analysis and Machine Intelligence*, 38(6):1155–1169, 2016. 1
- [25] M. Van den Bergh, X. Boix, G. Roig, B. de Capitani, and L. Van Gool. *SEEDS: Superpixels Extracted via Energy-Driven Sampling*, pages 13–26. Springer Berlin Heidelberg, 2012. 4
- [26] T.-C. Wang, A. A. Efros, and R. Ramamoorthi. Occlusion-aware depth estimation using light-field cameras. In *IEEE International Conference on Computer Vision*, pages 3487–3495, 2015. 2
- [27] T.-C. Wang, A. A. Efros, and R. Ramamoorthi. Depth estimation with occlusion modeling using light-field cameras. *IEEE Transactions on Pattern Analysis and Machine Intelligence*, 38(11):2170–2181, 2016. 3
- [28] T.-C. Wang, M.-Y. Liu, J.-Y. Zhu, A. Tao, J. Kautz, and B. Catanzaro. High-resolution image synthesis and semantic manipulation with conditional gans. *arXiv preprint arXiv:1711.11585*, 2017. 2
- [29] T.-C. Wang, J.-Y. Zhu, E. Hiroaki, M. Chandraker, A. A. Efros, and R. Ramamoorthi. A 4d light-field dataset and cnn architectures for material recognition. In *European Conference on Computer Vision*, pages 121–138. Springer, 2016. 1
- [30] T.-C. Wang, J.-Y. Zhu, N. K. Kalantari, A. A. Efros, and R. Ramamoorthi. Light field video capture using a learning-based hybrid imaging system. *ACM Transactions on Graphics*, 36(4):133, 2017. 1
- [31] S. Wanner and B. Goldluecke. Variational light field analysis for disparity estimation and super-resolution. *IEEE transactions on pattern analysis and machine intelligence*, 36(3):606–619, 2014. 2
- [32] G. Wu, M. Zhao, L. Wang, Q. Dai, T. Chai, and Y. Liu. Light field reconstruction using deep convolutional network on epi. In *Proceedings of the IEEE Conference on Computer Vision and Pattern Recognition*, pages 6319–6327, 2017. 1, 2
- [33] R. A. Yeh, C. Chen, T.-Y. Lim, A. G. Schwing, M. Hasegawa-Johnson, and M. N. Do. Semantic image inpainting with deep generative models. In *CVPR*, volume 2, page 4, 2017. 2
- [34] H. W. F. Yeung, J. Hou, J. Chen, Y. Y. Chung, and X. Chen. Fast light field reconstruction with deep coarse-to-fine modelling of spatial-angular clues. In *European Conference on Computer Vision*, 2018. 6, 7

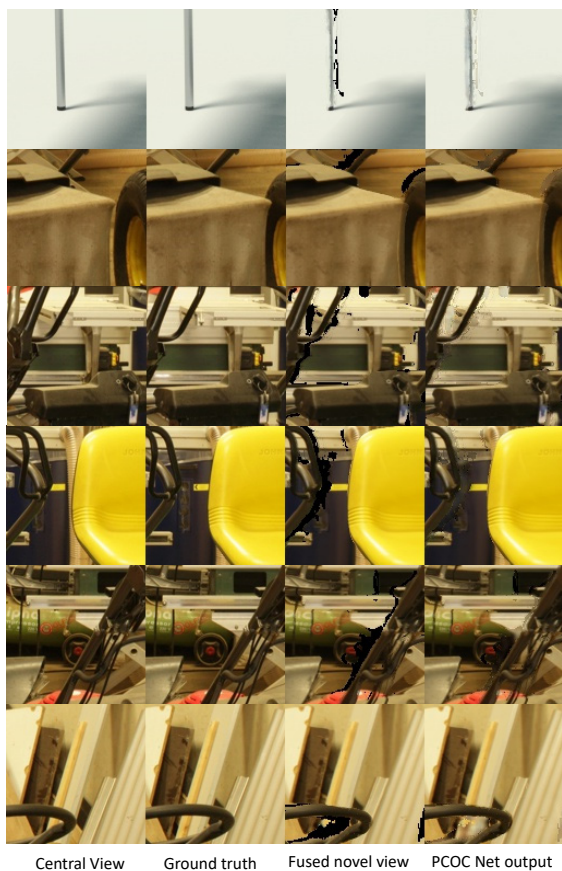


Figure 4: Parallax correction and occlusion prediction from different competing algorithms at different baseline expansion ratios ranging between 5 and 9.

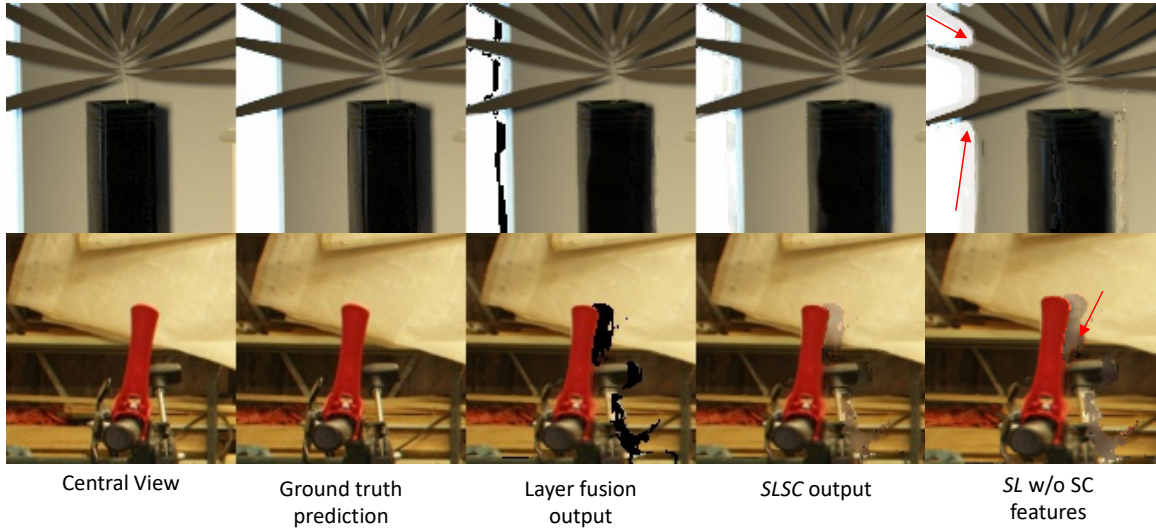


Figure 5: Network structure for the proposed *POC-Net*. The top row is extracted from view 31 of *Furniture1*, and view 71 of *Workshop*. Both with 5x baseline expansion.

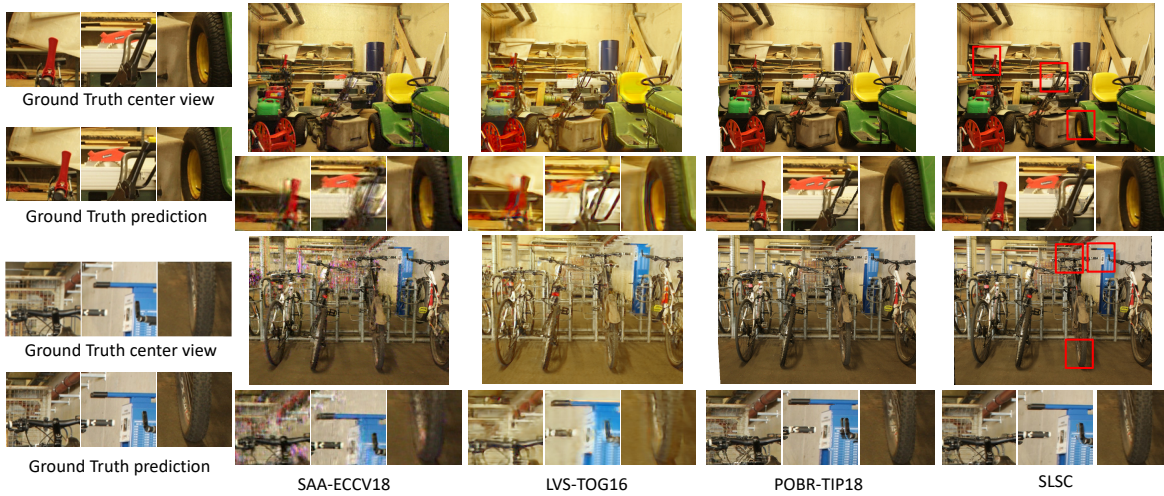


Figure 6: Network structure for the proposed *SLSC* model. The top row is extracted from view 21 of *Workshop*, and view 71 of *Bikes*, with baseline expansion ratio of 7.5x and 6x, respectively.